

# Enhancing the Thermoelectric Figure of Merit in Engineered Graphene Nanoribbons

Hatef Sadeghi\*, Sara Sangtarash and Colin J Lambert

Quantum Technology Centre, Department of Physics, Lancaster University, LA1 4YB Lancaster, UK

\* Corresponding author: Hatef Sadeghi – h.sadeghi@lancaster.ac.uk

## Abstract

We demonstrate that thermoelectric properties of graphene nanoribbons can be dramatically improved by introducing nanopores. In monolayer graphene, this increases the electronic thermoelectric figure of merit  $ZT_e$  from 0.01 to 0.5. The largest values of  $ZT_e$  are found when a nanopore is introduced into bilayer graphene, such that the current flows from one layer to the other via the inner surface of the pore, for which values as high as  $ZT_e = 2.45$  are obtained. All thermoelectric properties can be further enhanced by tuning the Fermi energy of the leads.

**Keywords:** Thermoelectric figure of merit, thermopower, thermal conductance, graphene nanoribbons, quantum transport

## 1. Introduction

Nowadays, the performance of nanoelectronic devices is limited by dissipated power rather than available clock speeds [1]. To address this issue, thermoelectric energy conversion may be an essential ingredient in the design of the next generation integrated electronics, optoelectronic and photonic devices [2]. On the one hand efficient thermoelectricity requires a strongly suppressed thermal conductivity ( $\kappa$ ) since the performance of thermoelectric devices is inversely proportional to the thermal conductivity. On the other hand, the cooling of local hot spots requires a high thermal conductivity [3]. Thermal conductance in a

solid is defined by Fourier's law,  $q = -\kappa \nabla T$  where  $q$  is the heat flux,  $\kappa = \kappa_{pl} + \kappa_e$  is the thermal conductance due to phonons ( $\kappa_{pl}$ ) and electrons ( $\kappa_e$ ) and  $\nabla T$  is the temperature gradient [1]. Although acoustic phonons are the main heat carriers in bulk crystals, nanostructures show significantly different thermal properties. This is due to the increased phonon–boundary scattering, changes in the phonon density of states and their dispersion in low dimensional semiconductors [2, 4-6].

The efficiency of a thermoelectric device and material is determined by its thermoelectric figure of merit ( $ZT = S^2GT/\kappa$ ) where  $S$  is Seebeck coefficient, which depends on the asymmetry of the density of states around the Fermi level,  $G$  is the electrical conductance and  $T$  is the temperature [7]. Similarly, the electronic thermoelectric figure of merit also is defined as:  $ZT_e = S^2GT/\kappa_e$ . Since the efficiency of a thermoelectric device can be enhanced by increasing the power factor ( $S^2GT$ ) or decreasing the thermal conductance, there is a need to simultaneously increase the Seebeck coefficient and electrical conductance, while reducing in thermal conductance. Since these factors are correlated, increasing  $ZT$  to values greater than unity is challenging. The most common material used in thermoelectric applications is bismuth and its alloys, which are toxic, expensive and have limit global supplies. To improve  $ZT$  in new materials, one promising route has been to take advantage of the reduced phonon thermal conductance ( $\kappa_{pl}$ ) in low dimensional materials [8]. In what follows we apply this approach to engineered graphene nanoribbons [9, 10] and show that introducing nanopores into bilayer graphene [11], a room-temperature  $ZT_e$  higher than 2 could be achieved.

## 2. Computational Methods

The electrical conductance  $G(T)$ , the electronic contribution to the thermal conductance  $\kappa(T)$ , the thermopower (Seebeck coefficient)  $S(T)$  and the Peltier coefficient  $\Pi(T)$  of a junction as a function of the temperature  $T$  can be obtained by calculating the transmission probability  $T(E)$  of the electrons with energy  $E$  passing from one electrode to another. From  $T(E)$ , in the linear response the quantity  $L_n(T)$  is defined as:

$$L_n(T) = \int_{-\infty}^{+\infty} dE (E - E_F)^n T(E) \left( -\frac{\partial f(E)}{\partial E} \right) \quad (1)$$

where  $f(E)$  is the Fermi-Dirac probability distribution function ( $f(E) = (1 + \exp(E - E_F/k_B T))^{-1}$ ),  $T$  is the temperature,  $e$  is electron charge and  $h$  is the Planck's constant and  $E_F$  the Fermi energy.

The electrical conductance  $G(T)$  as a function of the temperature  $T$  is then given by the Landauer formula  $G(T) = G_0 L_0(T)$  where  $G_0 = 2e^2/h$  is the conductance quantum. The electronic thermal conductance  $\kappa(T)$ , the Seebeck  $S(T)$  and Peltier  $\Pi(T)$  coefficients are also given by [12]:

$$\kappa(T) = \frac{L_0 L_2 - L_1^2}{h T L_0} \quad (2)$$

$$S(T) = -\frac{L_1}{e T L_0} \quad (3)$$

$$\Pi(T) = T S(T) \quad (4)$$

To find the optimized geometry and ground state Hamiltonian of the structure analogously as described in [9] we employed, we employed the SIESTA [13] implementation of DFT using the generalized gradient approximation (GGA) of the exchange and correlation functional with the Perdew-Burke-Ernzerhof parameterization (PBE) [14] a double zeta polarized basis set, a real-space grid defined with a plane wave cut-off energy of 250 Ry and a maximum force tolerance of 40 meV/Å. From the converged DFT calculation, the underlying mean-field Hamiltonian was combined with the GOLLUM [12] implementation of the non-equilibrium Greens function (NEGF) method. This yields the transmission coefficient  $T(E)$  for electrons of energy  $E$  (passing from the source to the drain) via the relation [15]

$$T(E) = \text{Trace} \{ \Gamma_R(E) G^R(E) \Gamma_L(E) G^{R\dagger}(E) \} \quad (5)$$

In this expression,  $\Gamma_{L,R}(E) = i(\Sigma_{L,R}(E) - \Sigma_{L,R}^\dagger(E))$  describe the level broadening due to the coupling between left (L) and right (R) electrodes and the central scattering region (S) associated with the pore.

$\Sigma_{L,R}(E) = H_{LS,RS}^\dagger G_{L,R} H_{LS,RS}$  are the retarded self-energies associated with this coupling.  $H_{LS,RS}$  and  $G_{L,R}$

are the coupling matrix between  $LS$  and  $RS$  and the surface Green's function of the electrodes, respectively.  $G^R = (ES - H_S - \Sigma_L - \Sigma_R)^{-1}$  is the retarded Green's function, where  $H_S$  is the Hamiltonian of the scattering region and  $S$  is overlap matrix.

### 3. Results and discussions

**3.1. Thermal properties of Graphene:** Carbon based materials show a wide range of thermal properties from  $\sim 0.01 \text{ WmK}^{-1}$  in amorphous carbon to above  $2,000 \text{ WmK}^{-1}$  at room temperature in graphene [1, 16-19] and even higher in few layer graphene [20]. This means that 2D graphene and its multilayer counterparts are useful for thermal management applications [21]. The high thermal conductivity of the graphene is mainly due to the high phonon contribution to heat transport. Therefore, for thermoelectricity applications, one needs to engineer phonon transport to achieve a low thermal conductivity. Moreover, graphene is a zero gap material and not suitable to use as thermoelectric material because of its very small Seebeck coefficient. However, theoretical studies revealed that phonon transport is sensitive to defects, strain, sample size and geometry [21] and it is known that by patterning graphene to form nanoribbons or anti dots one can suppress the phonon contribution to heat transport [3]. This suppression is supported by experimental data, as reviewed in ref. [2].

Phonon transport in graphene ribbons is limited by the ribbon size and edge characteristics [20]. In addition, equilibrium molecular dynamic simulations showed that hydrogen passivation of the graphene-nanoribbon edges reduces significantly the thermal conductivity [22, 23]. Anti-dots in graphene, one can further reduce the phonon thermal conductivity [8]. For example, anti-dots created by removing 2% of the total number of atoms in pristine graphene, reduced the phonon induced thermal conductivity by almost 50% [21]. However, the stability of antidots in graphene is an issue due to self-healing properties of the monolayer graphene [24].

Here we build upon these results by investigating the thermoelectric properties of various forms of engineered graphene, obtained by sculpting nanopores in bilayer graphene and allowing the pore surface to reconstruct [9]. Pores in bilayer graphene are not only more stable than anti-dots in monolayer graphene, but should also be effective in reducing the phonon contribution to thermal conductance. In what follows, we

explore the electrical conductance, thermal conductance, Seebeck and Peltier coefficients of the range of structures shown in fig 1. These engineered graphene ribbons include: a zigzag monolayer graphene nanoribbon with hydrogen terminated edges (fig. 1a), a monolayer graphene nanopore with hydrogen terminated edges (fig. 1b), an AA- bilayer graphene nanoribbon (fig. 1c), an engineered bilayer graphene nanopore (fig. 1d), an AA- bilayer graphene with monolayer lead, in which the transport takes place from the top layer to the bottom layer (fig. 1e), an engineered bilayer graphene nanopore with monolayer leads and either hydrogen termination [9] (fig. 1f) or oxygen termination (fig. 1g) inside the pore. The ribbon lengths and widths in all cases are almost equal ( $L \approx 6\text{nm}$ ,  $W \approx 3\text{nm}$ ) and the pores sizes are  $\approx 1.3\text{nm}$ .

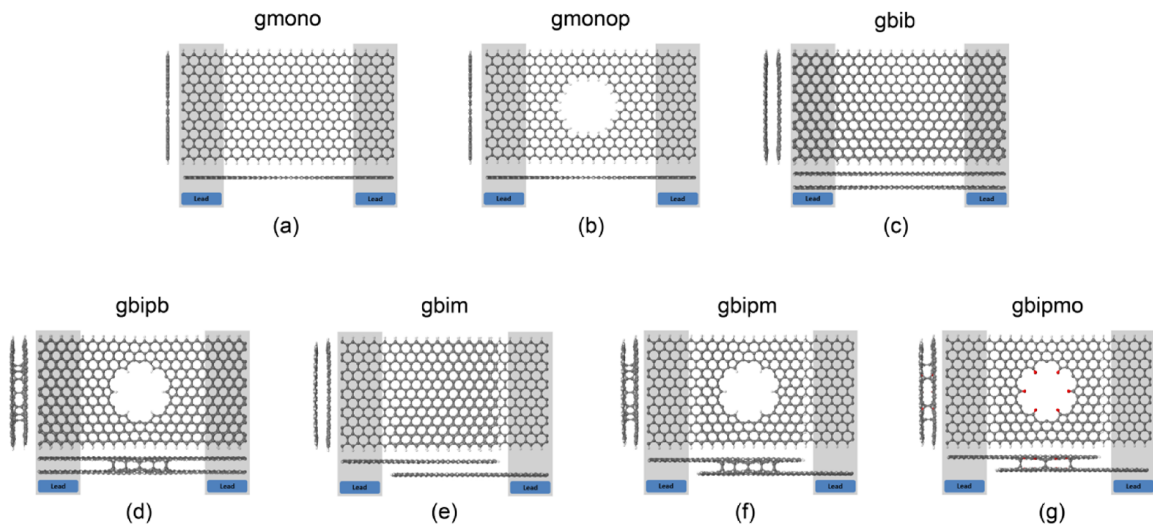


**Figure 1:** Geometry of the graphene-based structures, (a) monolayer graphene ribbon, (b) monolayer graphene nanopore, (c) AA- bilayer graphene ribbon, (d) Engineered bilayer graphene nanopore, (e) AA- bilayer graphene with monolayer lead, (f) Engineered bilayer graphene nanopore with monolayer lead and hydrogen termination inside the pore, (g) Engineered bilayer graphene nanopore with monolayer lead and oxygen termination inside the pore.

**3.2. Thermoelectric properties of a monolayer graphene nanoribbon and nanopores:** Figure 2 (a) shows the transmission coefficient  $T(E)$  for electrons with energy  $[-0.7, 0.7]$  eV transmitting from one side of the monolayer graphene nanoribbon and/or monolayer graphene nanopore to the other side. For a

perfect crystalline zigzag edge monolayer graphene nanoribbon with hydrogen terminated edges (fig. 1a-gmono),  $T(E)=1$  outside the Fermi energy and  $T(E)=3$  near the Fermi energy. The high  $T(E)$  near the Fermi energy is due to the edge states and band bending, as predicted theoretically [25] and observed experimentally [26-29].

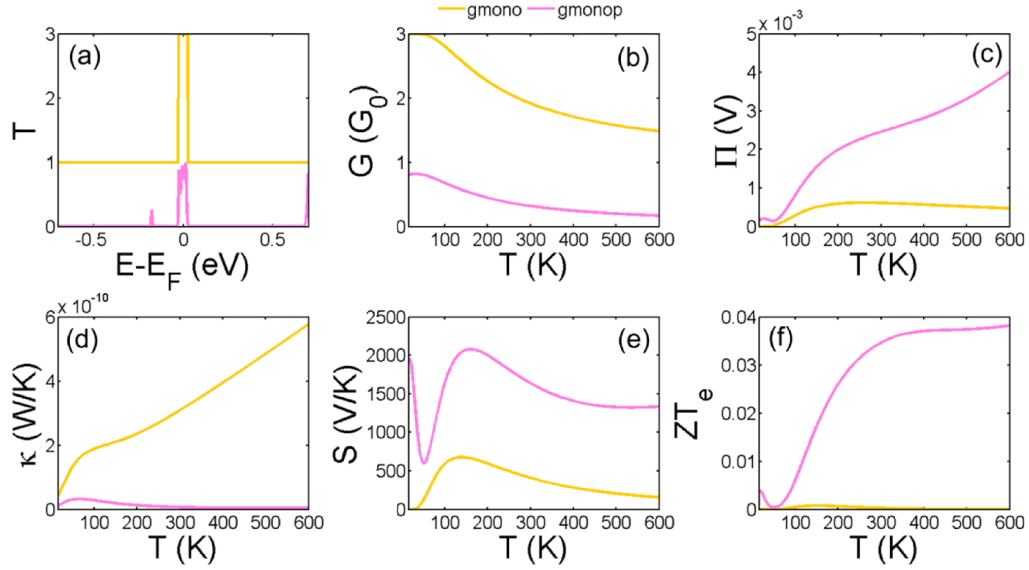


**Figure 2:** (a) Transmission coefficient  $T(E)$ , (b, c) electrical and thermal conductance ( $G$ ,  $\kappa$ ), (d, e) Peltier ( $\Pi$ ) and Seebeck ( $S$ ) coefficients and (f) figure of merit as a function of temperature in zigzag monolayer graphene nanoribbon (gmono) and monolayer graphene nanopore (gmonop).

By drilling a hole in the ribbon to create a nanopore as shown in fig. 1b,  $T(E)$  is modified to that shown in fig. 2a-gmonop (pink curve). In this case, the probability of transmitting electron with energies above or below the Fermi energy is suppressed due to the presence of the pore, whereas the high transmission feature in the vicinity of the Fermi energy still preserved. This improves the thermo-power (fig. 2e) by the factor of 4 and reduces the electronic thermal conductance significantly (fig 2d), leading to significant enhancement in the  $ZT_e$ . However, the  $ZT_e$  does not exceed 0.04 at room temperature which is not promising. This agrees with the results reported elsewhere [7].

**3.3. Thermoelectric properties of engineered bilayer graphene:** Figure 3a shows  $T(E)$  for the structures shown in fig. 1(c-g). The bilayer graphene nanoribbons with hydrogen terminated edges have the highest thermal conductance and lowest thermopower amongst all the examples of bilayer graphene. By connecting only the top layer of the left hand side to the left electrode and bottom layer of the right hand side to the right electrode (fig. 1f) so that the current flows through the surface of the pore coupling the top and bottom layers of the bilayer, the thermal conductivity is suppressed and  $ZT_e$  is improved but only at low temperatures.

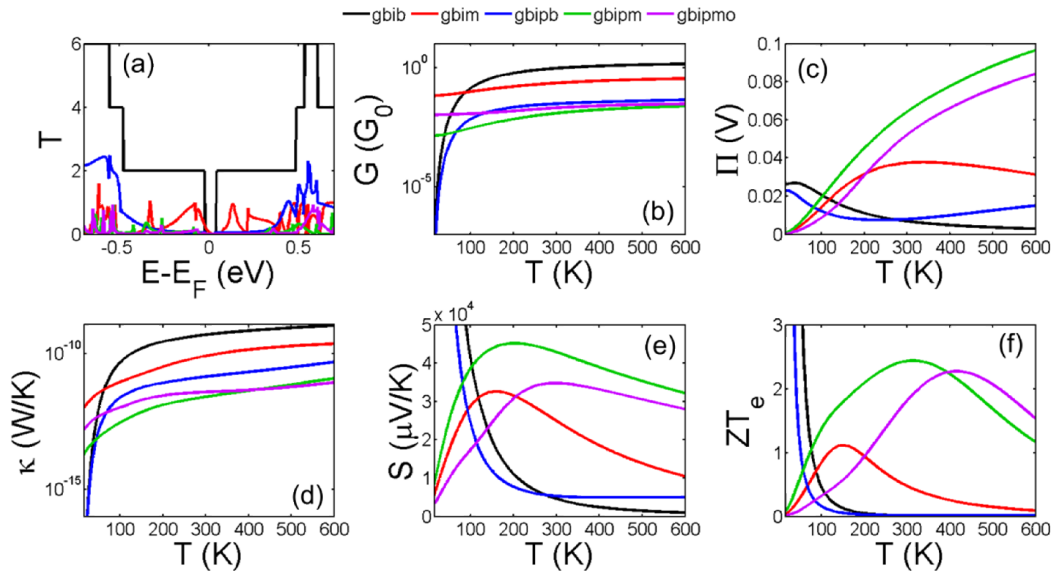


**Figure 3:** (a) Transmission coefficient  $T(E)$ , (b) electrical conductance ( $G$ ), (c) Peltier ( $\Pi$ ) coefficient, (d) thermal conductance ( $\kappa$ ), (e) Seebeck ( $S$ ) coefficient and (f) figure of merit as a function of temperature in zigzag bilayer graphene nanoribbon (gbib), bilayer graphene with monolayer lead (gbim), engineered bilayer graphene nanopore (gbipb), engineered bilayer graphene nanopore with monolayer lead and hydrogen termination in pore side (gbipm), engineered bilayer graphene nanopore with monolayer lead and oxygen termination in pore side (gbipmo).

By placing a hole in bilayer graphene and allowing it to be reconstructed, such that the pore edges couple the top and bottom layers, we find that the thermal conductance is significantly suppressed (fig 3d,e). This is even more pronounced for the bilayer nanopore with monolayer leads and hydrogen or oxygen terminations

in pore side (fig. 1f,g). As shown in fig. 3f, for both hydrogen and oxygen terminations, the high thermopower and low thermal conductance of this engineered bilayer graphene induces a significant increase in the room-temperature figure of merit ( $ZT_e \approx 2.5$ ).

To provide insight into the above improvements in  $ZT_e$ , we note that an asymmetric delta function-like peak in the transmission coefficient around the Fermi energy is known to have high  $ZT_e$  [4]. Here we show that the asymmetric step-function-like transmission coefficient  $T(E)$  will could lead to high  $ZT_e$ . Figure 4a shows a model ideal transmission coefficient in the form of a step function near  $E_F$ . Figure 4b-e shows corresponding electrical conductance ( $G$ ), thermal conductance ( $\kappa$ ), Seebeck ( $S$ ) coefficient and electronic figure of merit as a function of position of step function  $E_0$  and the amplitude  $A$ . It is apparent from figure 4e that by optimizing the location of the step  $E_0$  one could achieve a high  $ZT_e$ . By choosing the phononic contribution of thermal conductance about 5 times higher than the electronic contribution, figure 4f shows the full  $ZT$ .

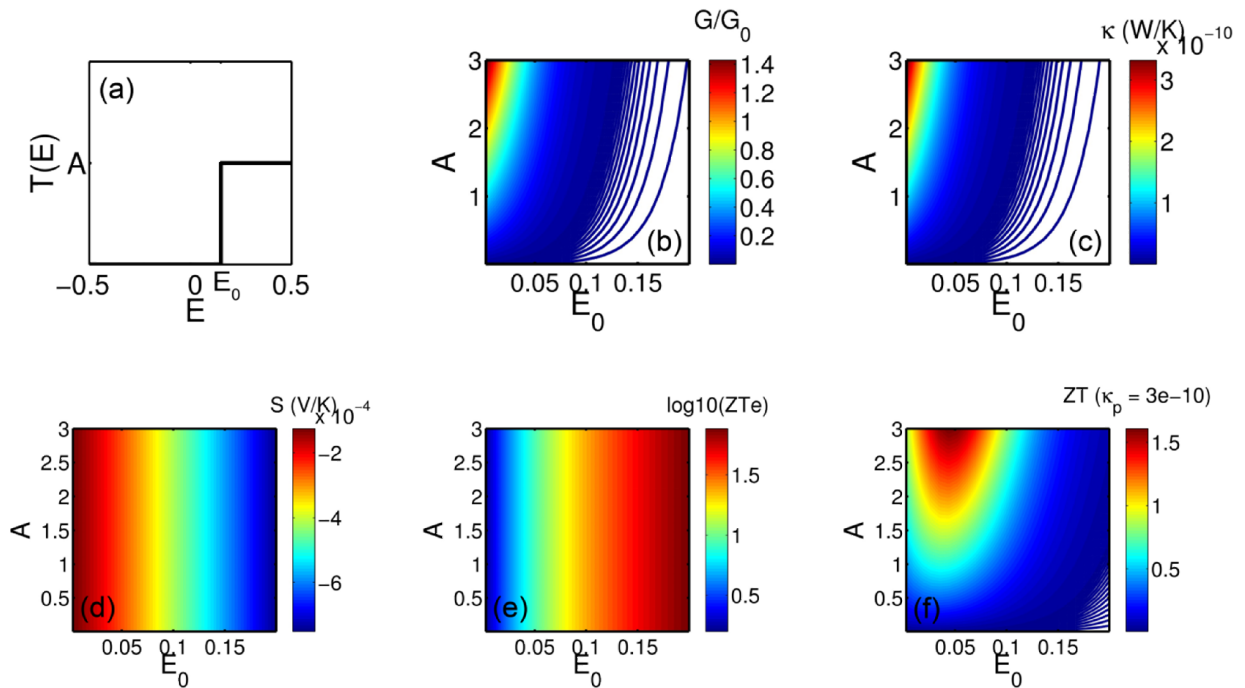


**Figure 4:** (a) Ideal step function like transmission coefficient  $T(E)$  asymmetric around Fermi energy ( $E=0$ ), (b) electrical conductance ( $G$ ), (c) thermal conductance ( $\kappa$ ), (d) Seebeck ( $S$ ) coefficient and (e) electronic and (f) full figure of merit as a function of position of step function  $E_0$  and the amplitude of  $T(E)$ .

For the structures in figure 3,  $T(E)$  possess gaps rather than step functions near  $E_F$ . However when these are placed asymmetrically relative to  $E_F$ , one step-edge of the gap dominates. This gap also needs to be asymmetric around the Fermi energy to deliver high thermopower. By introducing a nanopore in the bilayer graphene (gbipm, gbipb or gbipmo) or considering the transport in the vertical direction (gbim), this gap is obtained. Although transport in the vertical direction (gbim) increases the gap and makes it slightly asymmetric, the transmission steps are not large enough and or sufficiently asymmetric to overcome thermal broadening at higher temperatures, although such features do improve  $ZT_e$  in low temperatures. Introducing a pore in bilayer graphene with bilayer leads makes the gap too big and step is too far from the Fermi energy and therefore it leads to low  $ZT_e$ . However, for gbipm and gbipmo, much better optimization is achieved leading to high  $ZT_e$ . This shows how one could engineer the gap size and Fermi energy of a graphene based structure by simply mechanically engineering the bilayer graphene.

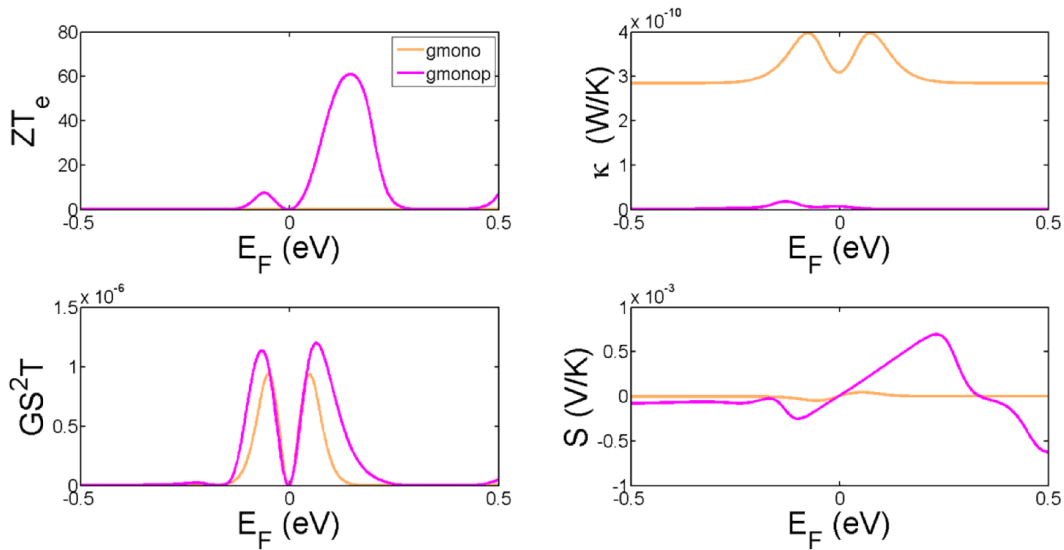


**Figure 5:** The variation of room-temperature values of  $ZT_e$ ,  $GS^2T$ ,  $S$  and  $\kappa$  as a function of Fermi energy  $E_F$  for a zigzag monolayer graphene ribbon (gmono) and a monolayer graphene nanopore (gmonop).

To further optimise the room-temperature thermoelectric properties of these structures, we now consider the effect of the tuning the Fermi energy. Figures 5 and 6 show the dependence on the Fermi energy of the room-temperature thermoelectric figure of merit  $ZT_e$ , the power factor  $GS^2T$ , the thermal conductance  $\kappa$  and

the Seebeck coefficient  $S$  of the structures shown in fig. 1. These demonstrate that by drilling a pore in both monolayer and bilayer graphene and tuning the Fermi energy,  $ZT_e$  is significantly improved. This improvement is much higher in monolayer graphene as shown in fig. 5 specifically at higher Fermi energies in the range of 0.1-0.2 eV, where the  $ZT_e$  improves by a factor of up to 60.

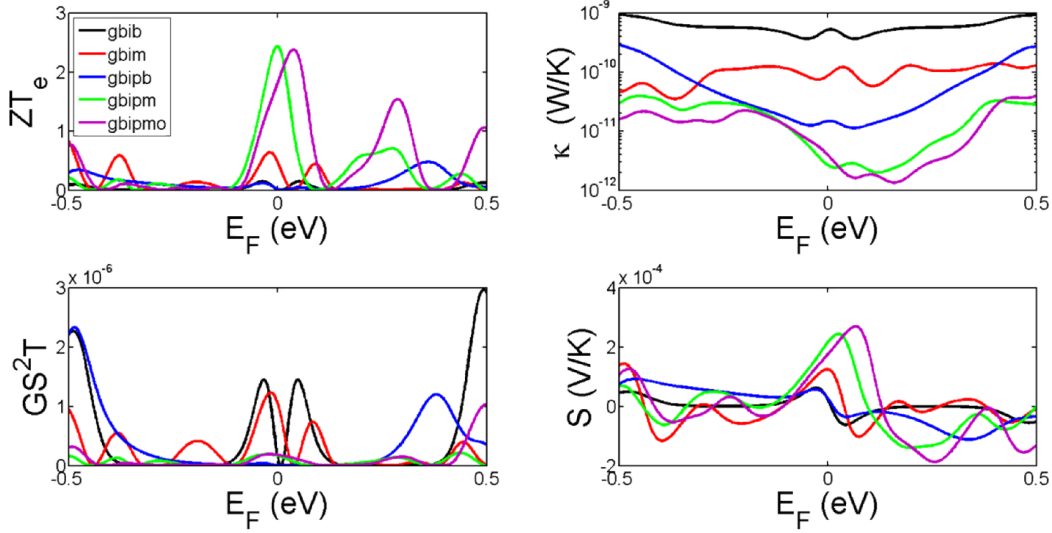


**Figure 6:** The variation of room-temperature values of  $ZT_e$ ,  $GS^2T$ ,  $S$  and  $\kappa$  as a function of  $E_F$  for zigzag bilayer graphene nanoribbon (gbib), bilayer graphene with monolayer lead (gbim), engineered bilayer graphene nanopore (gbipb), engineered bilayer graphene nanopore with monolayer lead and hydrogen termination in pore side (gbipm), engineered bilayer graphene nanopore with monolayer lead and oxygen termination in pore side (gbipmo).

#### 4. Conclusion

We have demonstrated two strategies for increasing  $ZT_e$  in bilayer graphene. First, by connecting the top graphene layer to a cold electrode and the bottom graphene layer to a hot electrode (fig. 1e), not only will the phonon contribution in thermal conductance be reduced due to the fact that the inter-layer coupling is weaker than the intra-layer C-C coupling, but  $ZT_e$  is increased by shifting the Fermi energy to the right (as in  $p$  doping) as it is clear by comparing the red and black curves in fig. 6. This improves  $ZT_e$  from 0.01 to 0.5 in  $E_F=0$ . The second strategy involves introducing pores in bilayer graphene. This shift and improvement of

$ZT_e$  is even higher when a pore is created in both layers, such that the top graphene layer is connected to the bottom graphene layer by the internal surface of the pore, as shown by green and purple curves in fig 6. This type of nanostructuring would also reduce the phonon contribution to the thermal conductance. By this technique the Fermi energy is shifted more to the left and  $ZT_e$  increases to 2.45 in the structure shown in figure 1f. Oxygen or hydrogen termination (fig. 1e,f) has a smaller effect in the  $ZT_e$  as shown in fig 5 green and purple curves. It is interesting to note that all bilayer structures possess a high thermopower in the range of 100s  $\mu$ V. Finally, figures 5 and 6 show that all thermoelectric properties can be further enhanced by tuning the Fermi energy of the leads.

## Acknowledgment

This work is supported by the UK EPSRC, EP/K001507/1, EP/J014753/1, EP/H035818/1, and from the EU ITN MOLESCO 606728

## References

1. Balandin, A.A., *Nat. Mater.* **2011**. 10(8): p. 569-581. doi: [10.1038/nmat3064](https://doi.org/10.1038/nmat3064)
2. Nika, D.L.; A.A. Balandin, *J. Phys.: Condens. Mat.* **2012**. 24(23): p. 233203. doi: [10.1088/0953-8984/24/23/233203](https://doi.org/10.1088/0953-8984/24/23/233203)
3. Karamitaheri, H.; M. Pourfath; R. Faez; H. Kosina, *IEEE Trans. Electron Devices* **2013**. 60(7): p. 2142-2147. doi: [10.1109/Ted.2013.2262049](https://doi.org/10.1109/Ted.2013.2262049)
4. Sadeghi, H.; S. Sangtarash; C.J. Lambert, *Sci. Rep.* **2015**. 5. doi: [10.1038/srep09514](https://doi.org/10.1038/srep09514)
5. Kambili, A.; G. Fagas; V.I. Fal'ko; C.J. Lambert, *Phys. Rev. B.* **1999**. 60(23): p. 15593-15596. doi: [10.1103/PhysRevB.60.15593](https://doi.org/10.1103/PhysRevB.60.15593)
6. Fagas, G.; A.G. Kozorezov; C.J. Lambert; J.K. Wigmore; A. Peacock; A. Poelaert; R. den Hartog, *Phys. Rev. B.* **1999**. 60(9): p. 6459-6464. doi: [10.1103/PhysRevB.60.6459](https://doi.org/10.1103/PhysRevB.60.6459)
7. Karamitaheri, H.; N. Neophytou; M. Pourfath; R. Faez; H. Kosina, *J. Appl. Phys.* **2012**. 111(5): p. 054501. doi: [10.1063/1.3688034](https://doi.org/10.1063/1.3688034)
8. Karamitaheri, H.; M. Pourfath; R. Faez; H. Kosina, *J. Appl. Phys.* **2011**. 110(5): p. 054506. doi: [10.1063/1.3629990](https://doi.org/10.1063/1.3629990)

9. Sadeghi, H.; L. Algaragholy; T. Pope; S. Bailey; D. Visontai; D. Manrique; J. Ferrer; V. Garcia-Suarez; S. Sangtarash; C.J. Lambert, *The Journal of Physical Chemistry B* **2014**. 118(24): p. 6908-6914. doi: [10.1021/jp5034917](https://doi.org/10.1021/jp5034917)
10. Sadeghi, H.; J.A. Mol; C.S. Lau; G.A.D. Briggs; J. Warner; C.J. Lambert, *Proc. Natl. Acad. Sci.* **2015**. 112(9): p. 2658–2663. doi: [10.1073/pnas.1418632112](https://doi.org/10.1073/pnas.1418632112)
11. Sadeghi, H.; M.T. Ahmadi; B. Ishak; S. Mousavi; R. Ismail, *Journal of Computational and Theoretical Nanoscience* **2011**. 8(10): p. 1993-1998. doi: [10.1166/jctn.2011.1915](https://doi.org/10.1166/jctn.2011.1915)
12. Ferrer, J.; C. Lambert; V. Garcia-Suarez; D. Zsolt Manrique; D. Visontai; L. Oroszlani; R. Ferradás; I. Grace; S. Bailey; K. Gillemot; H. Sadeghi; L. Algaragholy, *New J Phys* **2014**. 16: p. 093029. doi: [10.1088/1367-2630/16/9/093029](https://doi.org/10.1088/1367-2630/16/9/093029)
13. Soler, J.M.; E. Artacho; J.D. Gale; A. García; J. Junquera; P. Ordejón; D. Sánchez-Portal, *J. Phys.: Condens. Mat.* **2002**. 14(11): p. 2745. doi: [10.1088/0953-8984/14/11/302](https://doi.org/10.1088/0953-8984/14/11/302)
14. Perdew, J.P.; K. Burke; M. Ernzerhof, *Phys. Rev. Lett.* **1996**. 77(18): p. 3865-3868. doi: [10.1103/PhysRevLett.77.3865](https://doi.org/10.1103/PhysRevLett.77.3865)
15. Datta, S., *Quantum transport: atom to transistor*. **2005**: Cambridge Univ Pr.
16. Ghosh, S.; D.L. Nika; E.P. Pokatilov; A.A. Balandin, *New J Phys* **2009**. 11: p. 095012. doi: [10.1088/1367-2630/11/9/095012](https://doi.org/10.1088/1367-2630/11/9/095012)
17. Gunst, T.; T. Markussen; A.-P. Jauho; M. Brandbyge, *Phys. Rev. B*. **2011**. 84(15): p. 155449. doi: [10.1103/PhysRevB.84.155449](https://doi.org/10.1103/PhysRevB.84.155449)
18. Chang, P.-H.; B.K. Nikolic, *Phys. Rev. B*. **2012**. 86(4). doi: [10.1103/PhysRevB.86.041406](https://doi.org/10.1103/PhysRevB.86.041406)
19. Chang, P.-H.; M.S. Bahramy; N. Nagaosa; B.K. Nikolić, *Nano Lett.* **2014**. 14(7): p. 3779-3784. doi: [10.1021/nl500755m](https://doi.org/10.1021/nl500755m)
20. Balandin, A.A.; D.L. Nika, *Materials Today* **2012**. 15(6): p. 266-275. doi: [10.1016/S1369-7021\(12\)70117-7](https://doi.org/10.1016/S1369-7021(12)70117-7)
21. Karamitaheri, H.; N. Neophytou; M. Pourfath; H. Kosina, *J Comput Electron* **2012**. 11(1): p. 14-21. doi: [DOI 10.1007/s10825-011-0380-9](https://doi.org/10.1007/s10825-011-0380-9)
22. Evans, W.J.; L. Hu; P. Koblinski, *Appl. Phys. Lett.* **2010**. 96(20): p. 203112. doi: [10.1063/1.3435465](https://doi.org/10.1063/1.3435465)
23. Haskins, J.; A. Kinacı; C. Sevik; H. Sevinçli; G. Cuniberti; T. Çağın, *Acs. Nano*. **2011**. 5(5): p. 3779-3787. doi: [10.1021/nn200114p](https://doi.org/10.1021/nn200114p)
24. Zan, R.; Q.M. Ramasse; U. Bangert; K.S. Novoselov, *Nano Lett.* **2012**. 12(8): p. 3936-3940. doi: [10.1021/nl300985q](https://doi.org/10.1021/nl300985q)

25. Nakada, K.; M. Fujita; G. Dresselhaus; M.S. Dresselhaus, *Phys. Rev. B.* **1996**. 54(24): p. 17954-17961. doi: [10.1103/PhysRevB.54.17954](https://doi.org/10.1103/PhysRevB.54.17954)
26. Kobayashi, Y.; K.-i. Fukui; T. Enoki; K. Kusakabe; Y. Kaburagi, *Phys. Rev. B.* **2005**. 71(19): p. 193406. doi: [10.1103/PhysRevB.71.193406](https://doi.org/10.1103/PhysRevB.71.193406)
27. Niimi, Y.; T. Matsui; H. Kambara; K. Tagami; M. Tsukada; H. Fukuyama, *Phys. Rev. B.* **2006**. 73(8): p. 085421. doi: [10.1103/PhysRevB.73.085421](https://doi.org/10.1103/PhysRevB.73.085421)
28. Lahiri, J.; Y. Lin; P. Bozkurt; I.I. Oleynik; M. Batzill, *Nat. Nano.* **2010**. 5(5): p. 326-329. doi: [10.1038/nnano.2010.53](https://doi.org/10.1038/nnano.2010.53)
29. Jia, X.; M. Hofmann; V. Meunier; B.G. Sumpter; J. Campos-Delgado; J.M. Romo-Herrera; H. Son; Y.-P. Hsieh; A. Reina; J. Kong; M. Terrones; M.S. Dresselhaus, *Science* **2009**. 323(5922): p. 1701-1705. doi: [10.1126/science.1166862](https://doi.org/10.1126/science.1166862)